IOP Conf. Series: Materials Science and Engineering **352** (2018) 012018 doi:10.1088/1757-899X/352/1/012018

Pitting corrosion as a mixed system: coupled deterministic-probabilistic simulation of pit growth

Israr B M Ibrahim[1,2], S Fonna[2] and R Pidaparti[1]
[1]College of Engineering, University of Georgia, Athens, GA, US, 30622
[2]Corrosion and Computational Research Group (CCRG), Dept. of Mechanical and Industrial Engineering, Syiah Kuala University, Jl. Tgk. Syech Abdur Rauf No. 7 Darussalam, Banda Aceh, Indonesia 23111

E-mail: rmparti@uga.edu

Abstract. Stochastic behavior of pitting corrosion poses a unique challenge in its computational analysis. However, it also stems from electrochemical activity causing general corrosion. In this paper, a framework for corrosion pit growth simulation based on the coupling of the Cellular Automaton (CA) and Boundary Element Methods (BEM) is presented. The framework assumes that pitting corrosion is controlled by electrochemical activity inside the pit cavity. The BEM provides the prediction of electrochemical activity given the geometrical data and polarization curves, while the CA is used to simulate the evolution of pit shapes based on electrochemical activity provided by BEM. To demonstrate the methodology, a sample case of local corrosion cells formed in pitting corrosion with varied dimensions and polarization functions is considered. Results show certain shapes tend to grow in certain types of environments. Some pit shapes appear to pose a higher risk by being potentially significant stress raisers or potentially increasing the rate of corrosion under the surface. Furthermore, these pits are comparable to commonly observed pit shapes in general corrosion environments.

1. Introduction

Pitting corrosion is a destructive process that still poses a major problem in engineering. It is known to occur on stainless steel, and aluminum allows surface that has a protective layer on its surface. Failure to maintain this layer leads to a localized process of corrosion that digs into the depth of metals, and forms pits (and hence it is called pitting corrosion). These pits act as stress amplifier and lead to major failure [1-3]. Several case studies can be found describing the risk of pitting corrosion to engineering components such as boiler tube [4-5], steam turbine [6] and the major problem in aerospace engineering [7].

Pits can assume various shapes and densities. Shapes and densities are two parameters that are used to measure the severity of pitting corrosion [8]. The shapes and densities consequently also affect the stress distribution on metallic surfaces [9-13]. Pits can take various shapes depending on the environment and metal undergoing corrosion. Figure 1 shows some commonly observed pit shapes redrawn from [8].

Pitting corrosion occurs electrochemically, like in most metallic corrosion. The mathematical model of electrochemical reactions in corrosion is typically governed by Laplace equation. This model has been discussed extensively in numerous publications (among them are [14 – 17]). Boundary Element Method (BEM) is a popular choice for numerical method applied for corrosion model since it can be

used to compute solution only on the boundary (surface). Since corrosion is a surface phenomenon, this method saves a great deal of computational effort.

However, corrosion itself is a material-degrading process, and this becomes the main focus in pitting corrosion study as it seeks the shape evolution, that is pit cavity growth. A technique that is widely used for this problem is moving mesh method. Mai et al [18] have recently made a remarkable contribution to the modeling of pit cavity growth. In their study, pitting corrosion is seen from the multi-phase physics perspective. The two phases (the metal and corrosive substance) dynamically diffuse and the moving boundary can be conveniently described by the flux of diffusing ions (current density). The diverse shape of pit cavity in this model is induced by the irregularity of metallic grain influencing diffusion. In this study, moving mesh was incorporated into the model along with stochastic approach for pit cavity growth.

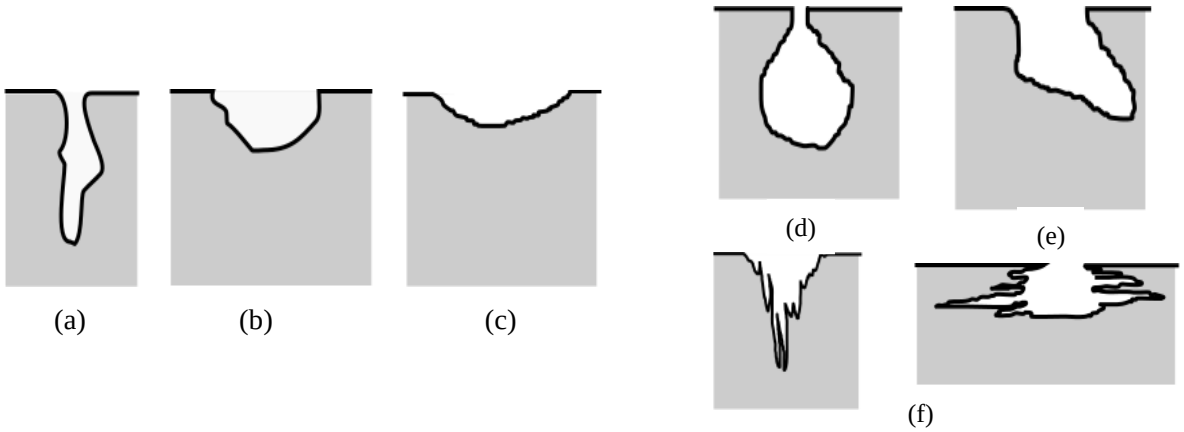

Figure 1. Some examples of common experimentally observed pitting shape, adapted from [3], (a) Narrow and deep, (b) Elliptical, (c) wide and shallow, (d) subsurface, (e) undercutting, (f) shapes influenced by microstructural orientation

Several previous works on pitting corrosion with the stochastic approach are available, including probabilistic model [19-20], Markov-based model [21] and Monte Carlo approach [22]. However, in this study, the electrochemical basis of corrosion was incorporated along with stochastic morphogenesis of pitting cavity. A well-known tool for the stochastic model is Cellular Automata (CA). CA is a method that has been used extensively for modeling non-linear system such as reaction diffusion [23], biological morphogenesis [24], the inflammatory response by immune cells [25-26]. These phenomena typically show stochastic impression at a smaller scale, but as the scale increases, they show apparent patterns. CA is widely used to model this behavior for its practicality in implementation. Several CA model for studying pitting corrosion is available as well. Pidaparti et al developed a CA that models the rate of spread a pit once initiated [27], including the interaction between pits in multi-pit growth [28]. However, this does not account for morphogenesis of pit cavity (growth in the depth direction). Li et al. [29] and di Caprio et al. [30] presented models on pit cavity growth in two- and three-dimensions. Their models are based on complete stochastics CA rules. This study incorporates established an electrochemical model of corrosion (as explained previously) into stochastic CA rules.

In this study, a framework for corrosion pit growth simulation based on the coupling of the Cellular Automaton and Boundary Element Method was developed. The framework assumes that pitting corrosion is controlled by electrochemical activity inside the pit cavity. The BEM provides a prediction of electrochemical activity given the geometrical data and polarization curves, while the CA is used to simulate the evolution of pit shapes based on electrochemical activity provided by BEM. An example case is presented to demonstrate the applicability of the developed framework.

2. Methods

The model in this study assumes that pitting is controlled by electrochemical activity inside the pit cavity, which is modeled using the BEM, while the CA is used to simulate the evolution of pit shapes based on electrochemical activity provided by BEM. Each of the aspects of BEM and CA is described below along with detailed information regarding how the coupling is carried out to achieve the pitting growth simulation.

2.1 Electrochemical Corrosion

In this study, it is assumed that electrochemical corrosion is the main driving force in the pitting corrosion process, and thus pitting growth. Pitting corrosion is assumed to be a particular electrochemical corrosion problem. This investigation is based on the electrostatic potential distribution that occurs on the metallic surface once electrochemical reactions of corrosion are established, and the growth of pits is stable. Because electrochemical reactions play the main role, the environmental condition is incorporated in the model as a polarization of electrochemical potential.

Pitting corrosion occurs on a metal that forms a passive layer that prevents the metal surface from interacting chemically with its environment. Once an area of passive layer breaks down, a portion of the metallic surface is exposed to the environment, and electrochemical reactions occur in this area. This area can be seen as a local corrosion cell. The surrounding area of the corrosion cell is highly passive; hence the corrosion cell that forms pitting can be seen as similar to a cathodic protection system where the pit area acts as the anode. Hence in this study, pitting corrosion is modeled as an electrochemical system governed by Laplace's equations (Figure 2) with three boundary conditions:

$$\phi = f_1(i) \qquad \text{at } \Gamma_1 \tag{1}$$

$$\phi = f_2(i) \qquad \text{at } \Gamma_2 \tag{2}$$

$$i = 0 \qquad \text{at } \Gamma_3 \tag{3}$$

Where ϕ is electrostatic potential (V), f_1 and f_2 are experimentally determined functions that account for polarization phenomenon, and i is current density (m/A^2). The current density follows the definition of flux of field ϕ,

$$i = \kappa \frac{\partial \phi}{\partial \mathbf{n}} \tag{4}$$

where κ is conductivity (1/Ω.m), and $\boldsymbol{n}$ is the normal vector.

The Laplace's equation is solved using BEM by following a scheme explained in [31]. By using BEM, the surface of a model is discretized into elements. In this study, only the two-dimensional model is considered. Hence constant line elements are used. However, the CA discretizes the domain into grids of uniform square cells. Thus, to couple the computational power of the two methods, an interface is necessary to be developed which will be explained later.

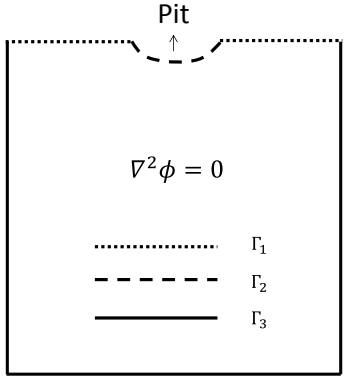

Figure 2. A cross-section of a metallic body undergoing pitting corrosion modeled as a domain governed by Laplace's equation

2.2. The Cellular Automata

Cellular Automata (CA) is a model that consists of a lattice of discrete, identical finite-state machines that evolves by a set of transition rules. The CA models dynamics of the system regarding discrete space and time. Hence, a cell in CA evolves only by transition rules to itself and cells in the vicinity (neighborhood). Each cell has its state, which is the binary state in early development, but can be represented in real numbers as well allow modeling of physical phenomena [23] such as diffusion. Several neighborhood schemes are available, but Moore and Neumann neighborhood [23] are typically used. The CA implementation in this study is explained below.

The CA grid in this study consists of rectangular or square cells with uniform size arranged to form the model. Hence, to accommodate these two approaches of discretization, a scheme is needed to interface the results provided by the two methods. In this study, the BEM line elements are used directly to construct the CA grid by taking the dimension of line elements as the dimensions of the squares that compose the CA grid. Hence, the BEM line elements are generated with uniform size. To generate the BEM line elements from the CA grid, the dimension of the uniform squares that build up the CA grid are taken as the dimension of the line elements. Figure 3 illustrates this approach in synchronizing both discretizations of the domain.

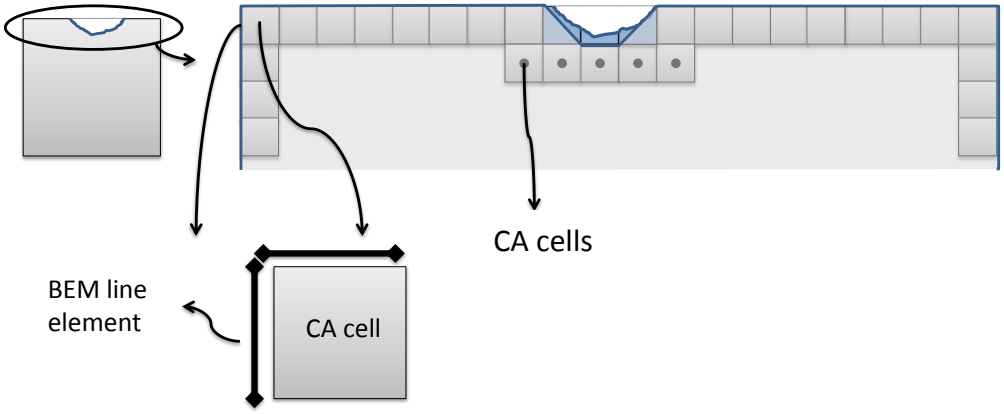

Figure 3. Coupling strategy adopted in CA and BEM

In this study, it is assumed that pit shape evolution is influenced by the electrochemical activity of the local corrosion cell. Hence, the potential distribution over the surface of the local corrosion cell is assumed to play the main role. However, the pit initiation and the path of pit growth are uncertain. In this case, the CA is used to compute the probability of initiation of new pits and the way it grows, based on the condition of the local corrosion cell. In this study, only potential distribution is considered as a major factor in determining the probability of initiation of pits and its growth.

To apply this mechanism, each cell in CA is assigned with three states representing the cathode, anode and the passive state. These can be encoded into integers. The corresponding potential value of a BEM line element is used to calculate the probability of the cell to change state. The influence of a neighboring cell is represented by summing the corresponding potential values of a cell with its neighboring cell's corresponding potential value.

The cathode cells with lower sum-of-potentials have higher chances of changing into anodes. This corresponds to viewing the pitting corrosion as a cathodic protection system, where a minimally protected area of a cathode can still undergo self-corrosion. The passive-state cells represent the subsurface body of the metal. Since corrosion occurs only on the surface, these cells have a higher chance of turning into cathodes or anodes, depending on which neighboring cells exerts the most influence on these cells. The influence is again represented by summing up all the potential values of the neighboring cells. The above-mentioned rules are implemented as below.

1. The anode cells will always be removed (corroded and converted into corrosion product) after each time iteration. If there is any non-electrode cell that shares a boundary with anode cells, then the states of anode cell are transferred into the cell.
2. The cathode and passive-state cells randomly change state into the anode. The chance is calculated as follow,

Cathode cells
$$S_{i+1} = \frac{\sum_{k,l=1}^{N} S_{i_{k,l}}}{m \times N_{cathode} \times E_{corr}} \quad (5)$$

Passive-state cells
$$S_{i+1} = \frac{m \times E_{corr}}{\sum_{k,l=1}^{N} S_{i_{k,l}}} \quad (6)$$

where,

S = Potential value from BEM simulation (V)
E_{corr} = Corrosion potential of cathode or anode (V)
m = number of electrode neighbors
$N\_cathode$ = number of cathode cells
k, l = index of cell and its neighbors

The cathode area is assumed to be highly passive. Once the pit grows, the cathode area reduces and increases the chance of the area to start corroding and grow pits. The neighborhood scheme used in this study is the Moore neighborhood. In this study, the surface is allowed to have multiple pits in this way so that it will consist of original pit growing in its original location and new pits growing and surrounding it. It is to be noted that equation (5) and (6) governs the evolution of the state of the discretization grid (as a "cathode", "passive"), and hence dimensionless.

2.3. Coupling the CA and BEM

The simulation is done iteratively. The BEM computation of potential distribution is carried out for a given domain at each iteration. The computation results (the potential distribution) are then delivered to CA as the basis to compute the rules. Between each execution of BEM and CA, an interface is needed to deliver the data into and from both discretizations. In this study, the discretization of BEM directly corresponds to the CA grid, and thus the line elements of BEM are uniform in size since CA consists of uniform square cells. The overall modeling methodology including the coupling of CA and BEM procedure is shown in Figure 4.

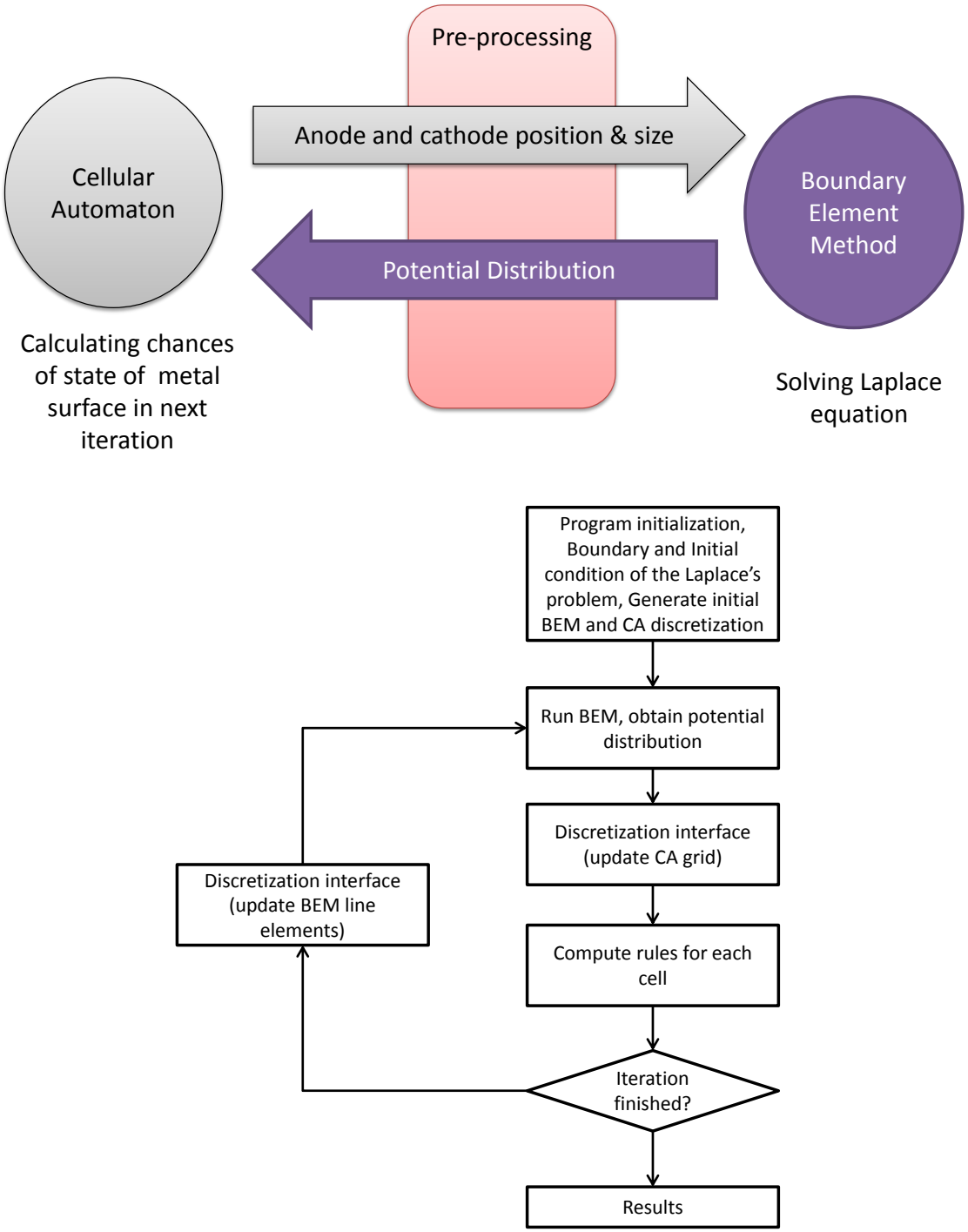

Figure 4. Procedure of the methodology for pitting growth simulation

3. Results and Discussion

A simple case is considered to demonstrate the proposed framework for pitting growth simulation. This case only considers a small localized site on which pitting was already initiated. When a pit initiates, it forms a region of cathode and anode. The anode area is smaller than the cathode area. It is assumed that the current exchange between anode and cathode takes place uniformly in and on the system. Thus, the corrosion cell formed can be modeled as a two-dimensional rectangular area as shown in Figure 5.

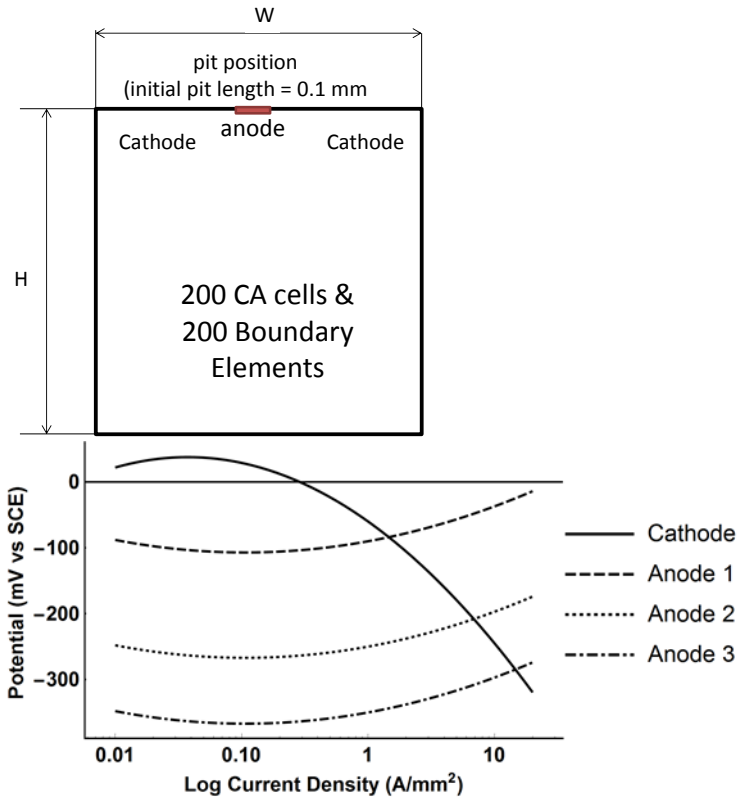

Figure 5. Left: Model of pitting corrosion simulation, unit is in mm. Right: Plot of polarization function 1, 2 and 3.

The simulation was done with different polarization functions that represent the corrosion cell behavior in specific environments, and different widths, W and depths, D, of the region. The width and depth of the region determine the area that currents will have to travel once a corrosion cell is formed. The dimensions are varied into 5x5, 10x10 and 20x20 mm for width x depth. The boundary condition of initial iteration is as in Equation 1,2 and three where the location of the initial pit is assigned as boundary Γ_2. The length of the initial pit is 0.1 mm. The polarization functions used as boundary condition Equation 2 and 3 are as shown in equation (7), (8) and (9), and plotted in Figure 5.

1
$$\begin{aligned}\text{Cathodic: } \phi_c &= -48\,\text{Log}^2(i) - 137\,\text{Log}\,(i) - 60 \\ \text{Anodic: } \phi_a &= 18\,\text{Log}^2(i) + 35\,\text{Log}\,(i) - 90\end{aligned} \tag{7}$$

2
$$\begin{aligned}\text{Cathodic: } \phi_c &= -48\,\text{Log}^2(i) - 137\,\text{Log}\,(i) - 60 \\ \text{Anodic: } \phi_a &= 18\,\text{Log}^2(i) + 35\,\text{Log}\,(i) - 250\end{aligned} \tag{8}$$

3
$$\begin{aligned}\text{Cathodic: } \phi_c &= -48\,\text{Log}^2(i) - 137\,\text{Log}\,(i) - 60 \\ \text{Anodic: } \phi_a &= 18\,\text{Log}^2(i) + 35\,\text{Log}\,(i) - 350\end{aligned} \tag{9}$$

Where ϕ_c is cathode potential (V), ϕ_a is anode potential (V), and i is current density (A/m^2). Polarization function 2 (Equation (8)) is an approximation of polarization of corrosion potential measured in [17]. The rest of the polarization functions are modifications of polarization function 2 to show the effect of variations of polarization in the example case. Figure 5 also shows a plot of the polarization functions. The cathodic polarization function is kept the same while the anode polarization is varied, so it has a larger difference from that of the cathode, thus making the corrosion cell more corrosive. It can also be seen that polarization curves I have lower corrosion current than the rest. As for conductivity κ, it is

treated a unity. Conductivity reflects environmental parameter. However, polarization curves (Equation (7), (8) and (9)) have incorporated environmental conditions in this model.

A series of simulation was done for various dimension and polarization curves. Each case consists of 5 trials of simulation. The number of pitting cases and the ratio of width over depth values obtained from the simulation are averaged. Results of the simulations showed that each polarization curve leads to different pit cavity properties. Figure 6 shows the width-to-depth ratio of pit cavity formed by all polarization curves with different corrosion cells. It shows that polarization curve 1 tends to lead to a higher width-to-depth ratio of pits despite corrosion cell size, while the smallest ratio is generated by polarization curve III. This means that pits in environments represented by polarization I lead to a wider opening of pits, while polarization curve III produces pits with a narrower opening. This provides a commonly used measure of pit width-depth ratio, but does not tell us anything about its shape. However, it shows a consistent geometrical trend in the simulation.

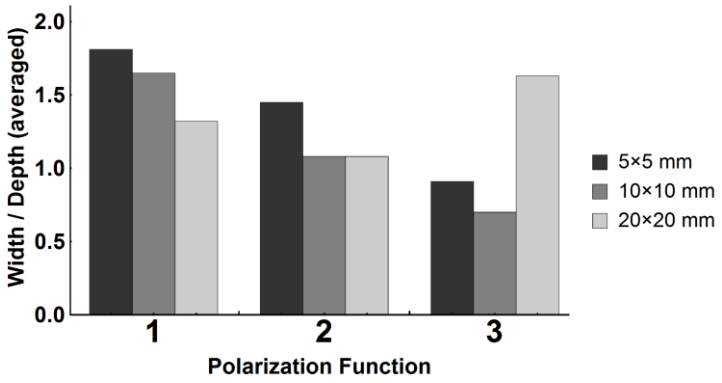

Figure 6. The width-to-depth ratio of pits formed in simulation after t=10 iterations.

Figure 7 shows samples of pit cavity shapes with a corrosion cell size of 5x5 mm in all three polarization curves. It shows the original pit shape after the 15th iteration at the center of the top of the rectangular model and new pits are formed on its right and left. It also shows that Polarization curve 1 tends to produce a conical pit, while polarization curves 2 and three show increasing irregularity of pit cavity shapes.

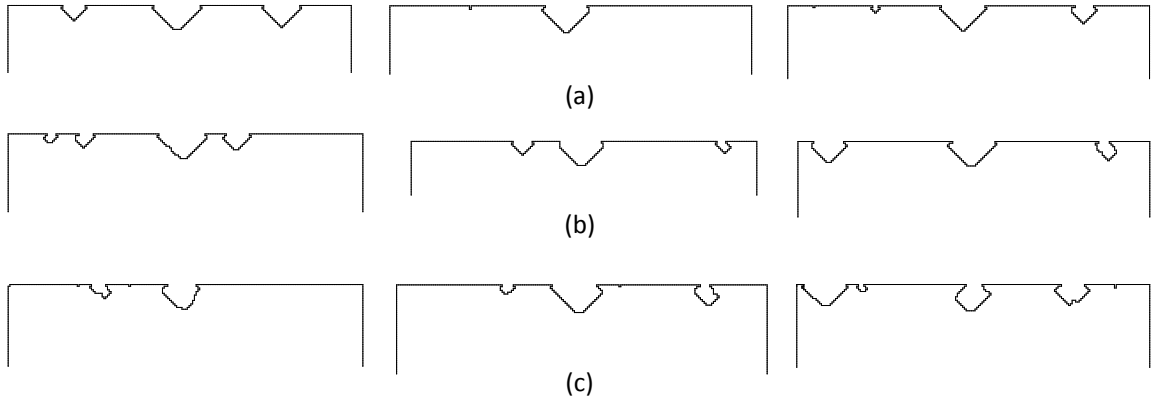

Figure 7. Three samples of pit shape produced at 15th iteration under polarization function (a) 1, (b) 2 and (c) 3

Pit cavity shapes generated by polarization one curve show consistent regular conical shapes despite repeated iterations and trials. However, when the corrosion cell size was increased, polarization 1 produced a more irregular conical pit shape, as shown in Figure 8. This result suggests that the corrosion cell size generated by pitting initiation can also influence pit growth.

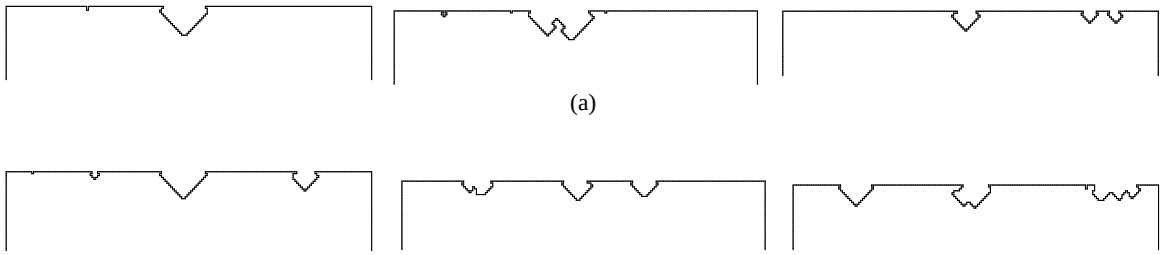

Figure 8. Three samples of pit shape produced at 15th iteration under polarization 1 with corrosion cell size of (a) 10x10 mm and (b) 20x20 mm.

Polarization curves 2 and 3 produced pit shape that tends to grow under the surface. Figure 9 shows a few samples of these pit cavity shapes. These pit shapes may behave differently than the regular conical or elliptical pit shapes since they provide room to accumulate active substance inside the pit and thus lead to the easier generation of subsurface pits. Furthermore, irregular shapes that result from branching inside the subsurface pit may generate higher stress concentrations inside the pit than the regular shapes. Assuming that pitting corrosion initiation is unavoidable, our results show that pits produced by polarization I are safer than ones that are produced by polarization III.

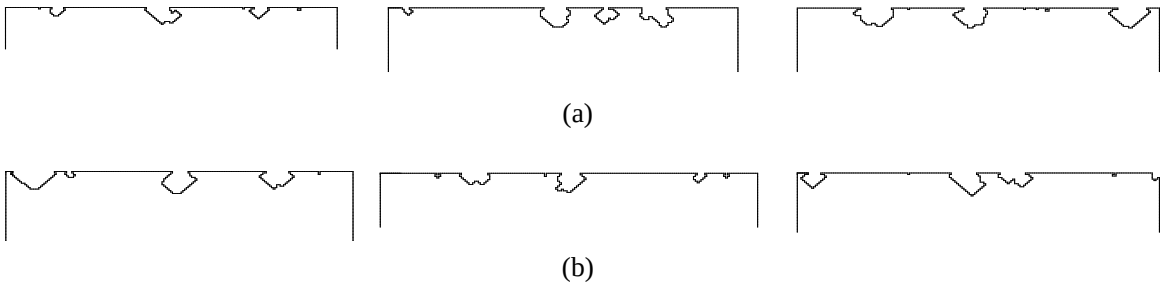

Figure 9. Three samples of pit shape produced at 15th iteration under polarization (a) 2 and (b) 3.

Figure 10 shows only the original pit and its growth from the first iteration to the 15th. It shows typical pits that are produced by in this study. In Figure 10(a), the growth (under polarization 1) shows a consistency of conical shape from the first iteration. This resembles commonly observed conical or elliptical pit shapes, such as illustrated in Figure 1(b) or (c). In Figure 10(b), the pit grew under polarization 3. The pit was initially conical in shape, but then the tendency changed toward subsurface growth. Figure 10(c) shows pit growth (under polarization 3) that was initially elliptical but then grew to a subsurface pit with a narrow opening. This pit grew to resemble the subsurface pit in Figure 1(d). Furthermore, some pits dug into the subsurface of the metal preferentially in a particular direction such as shown in Figure 10(d) and Figure 1(e). Hence, it has been shown that pits can assume different shapes based on the behavior of the local corrosion cell formed by pitting corrosion initiation.

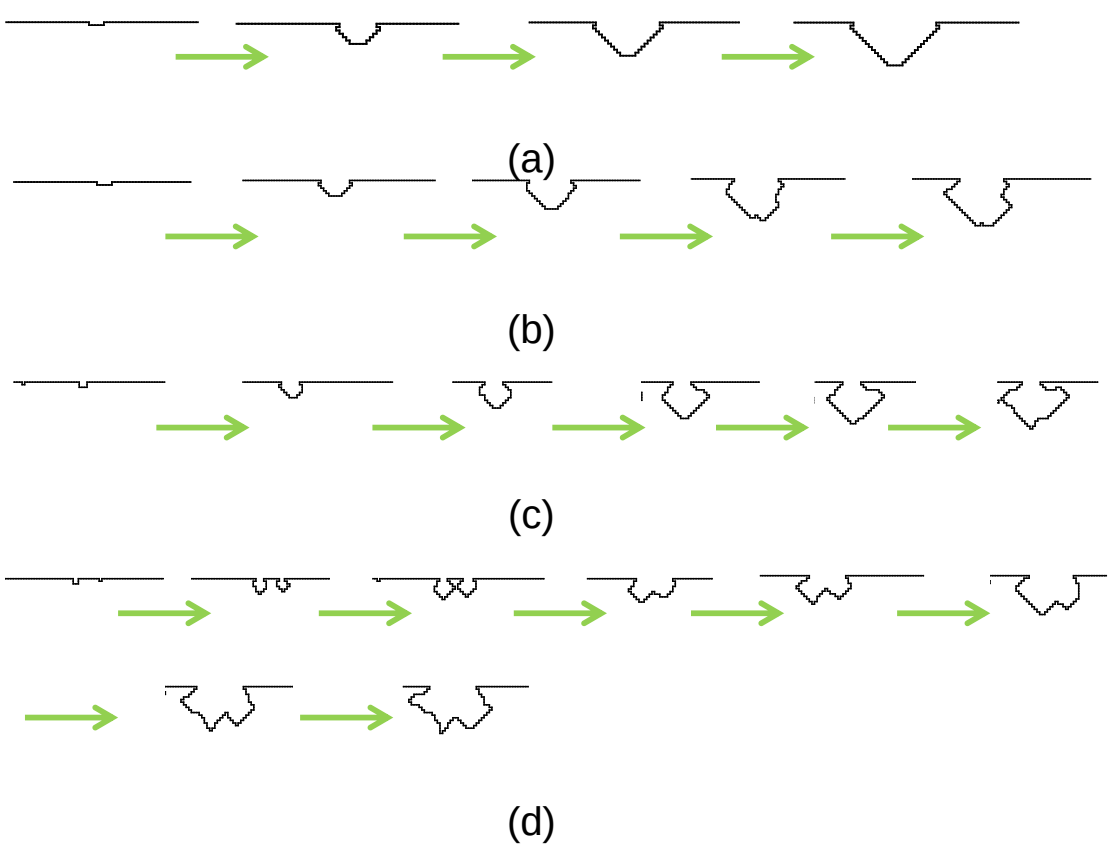

Figure 10. Growth of original pits under (a) polarization 1 with corrosion cell dimensions of 5x5 mm (b) polarization 3 with corrosion cell dimensions of 5x5 mm and (c) 10x10 mm, and (d) 20x20 mm

4. Concluding Remarks

In this study, pit cavity growth was treated as a stochastic event in which deterministic electrostatic model act as the probability distribution. The main finding in this study is that the more corrosive pit cavity increases the chance to produce subsurface pit (depicted in Figure 1(d)). Simulation results suggest that corrosion system with polarization functions 1 (the least corrosive among other two functions) is more likely to produce pit with a high width-to-depth ratio, or similar to an "elliptical" pit (Figure 1(b)). The corrosion system with polarization functions 3 (the most corrosive among the three) is more likely to develop pits with a lower width-to-depth ratio. As shown in Figure 11(c) and (d), these pits are similar to subsurface pits, where cavity continue to grow underneath the surface. These conclusions may not be generalized to every case of pitting corrosion. The experiment designed to measure correlation pit morphologies and potential distribution for a specific case (the type of materials and solutions) is needed to improve and validate the model. This is a planned future study.

Acknowledgements

The first author thanks the Fulbright Foundation for supporting his studies at VCU. RP thanks the US National Science Foundation for partially supporting the research through a grant DMR-0505039.

References

[1] Szklarska-Smialowska Z 2005 *Pitting and Crevice Corrosion* NACE International

[2] Rokhlin S I, Kim J-Y Nagy H, Zoofan B 1999 Effect of pitting corrosion on fatigue crack initiation and fatigue life *Eng. Fracture Mechanics* **62** 425–444
[3] Sankaran K K, Perez R and Jata K 2001 Effects of pitting corrosion on the fatigue behavior of aluminum alloy 7075-T6: modeling and experimental studies *Mater. Sci. Eng. A* **297** 223–229
[4] Heyes A M 2001 Oxygen pitting failure of a bagasse boiler tube *Engineering Failure Analysis* **8** 123–131
[5] Turnbull A and Zhou S 2004 Pit to crack transition in stress corrosion cracking of a steam turbine disc steel *Corrosion Science* **46** 1239–64
[6] Pantazopoulos G, Vazdirvanidis A, Tsinopoulos G 2011 Failure analysis of a hard-drawn water tube leakage caused by the synergistic actions of pitting corrosion and stress–corrosion cracking *Engineering Failure Analysis* **18** 649–57
[7] Hoeppner D W and Arriscorreta Carlos A 2012 Exfoliation corrosion and pitting corrosion and their role in fatigue predictive modeling: State-of-the-art review *International Journal of Aerospace Engineering* **2012**
[8] Frankel G S 2003 Corrosion: Fundamentals, Testing, and Protection *ASM Handbook* ASM International **13**A 236–41
[9] Pidaparti R M and Patel Ronak R. 2008 Correlation between corrosion pits and stresses in Al alloys *Materials Letters* **62** 4497-99
[10] Pidaparti R M, Rao S A 2008 Analysis of pits induced stresses due to metal corrosion *Corrosion Science* **50** 1932–38
[11] Turnbull A and L Crocker L Wright 2010 New insight into the pit-to-crack transition from finite element analysis of the stress and strain distribution around a corrosion pit *Corrosion Science* **52** 1492–98
[12] Cerit M, Genel K, and Eksi S 2009 Numerical investigation on stress concentration of corrosion pit, Engineering Failure Analysis, Volume **16** 2467–72
[13] Acuña N, González-Sánchez J, Kú-Basulto G and Domínguez L 2006 Analysis of the stress intensity factor around corrosion pits developed on structures subjected to mixed loading *Scripta Materialia* **55** 363–366
[14] Brebbia C A and Magureanu R 1987 The boundary element method for electromagnetic problems *Engineering Analysis* **4** 178–185
[15] Aoki S and Amaya K 1997 Optimization of cathodic protection system by BEM *Engineering Analysis with Boundary Elements* **19** 147–156
[16] Fonna S, Huzni S, Ridha M and Ariffin A K 2013 Inverse analysis using particle swarm optimization for detecting corrosion profile of rebar in concrete structure *Engineering Analysis with Boundary Elements* **37** 585-593
[17] Fonna S, Ibrahim I M, Ridha M, Huzni S, and Ariffin A K 2016 Simulation of the Ill-Posed problem of reinforced concrete corrosion detection using boundary element method *International Journal of Corrosion* **2016**
[18] Mai W, Soghrati S and Buchheit R G 2016 A phase field model for simulating the pitting corrosion *Corrosion Science* **110** 157-166
[19] Ahammed M and Melchers R E 1995 Probabilistic analysis of pipelines subjected to pitting corrosion leaks *Engineering Structures* **17**74–80
[20] Yuan X-X, Mao D, Pandey M D 2009 A Bayesian approach to modeling and predicting pitting flaws in steam generator tubes *Reliability Engineering & System Safety* **94** 1838–1847
[21] Valor A, Caleyo F, Alfonso L, Velázquez J C, And Hallen J M 2013 Markov chain models for the stochastic modeling of pitting corrosion *Mathematical Problems In Engineering*
[22] Caleyo F, Velázquez J C, Valor A and Hallen J M 2009 Probability distribution of pitting corrosion depth and rate in underground pipelines: A Monte Carlo study *Corrosion Science* **51** 1925–1934
[23] Schiff J L 2007 *Cellular Automata, A Discrete View Of The World* (Wiley Interscience)

[24] Ermentrout G B and Edelstein-Keshet L 1993 Cellular automata approaches to biological modeling *J. Theor. Biol* **160** 97–133
[25] Ibrahim I, Oruganti S V and Pidaparti R 2017 Simulation of healing threshold in strain-induced inflammation through a discrete informatics model *IEEE J. Biomed. Heal. Informatics* 1–1
[26] Aghasafari P, Ibrahim I B M and Pidaparti R 2017 Strain-induced inflammation in pulmonary alveolar tissue due to mechanical ventilation *Biomech. Model Mechanobiol* **16**
[27] Pidaparti R M, Palakal M J and Fang L 2004 Corrosion pit growth model using cellular automata *AIAA Journal* **42** 2562-2569
[28] Pidaparti R M, Fang Long and Palakal M J 2008 Computational simulation of multi-pit corrosion process in materials *Computational Materials Science* **41** 255–265
[29] Lei Li, Xiaogang Li, Chaofang Dong and Yizhong Huang 2009 Computational simulation of metastable pitting of stainless steel *Electrochimica Acta* **54** 6389–6395
[30] Di Caprio D, Vautrin-UI C, Stafiej J, Saunier J, Chausse A, Feron D and Badiali J P 2010 Morphology of corroded surfaces: Contribution of cellular automaton *Modelling Corrosion Science* **53** 418-425
[31] Aoki S and Kishimoto K 1991 Prediction of galvanic corrosion rates by the boundary element method *Mathematical and Computer Modelling* **15** 11–22